A Scanning Frequency Mode for Ion Cyclotron Mobility Spectrometry

3 AUTHORS, INCLUDING:

Rebecca S Glaskin
Boston University
3 PUBLICATIONS **95** CITATIONS

SEE PROFILE

Stephen Valentine
West Virginia University
78 PUBLICATIONS **3,235** CITATIONS

SEE PROFILE

A Scanning Frequency Mode for Ion Cyclotron Mobility Spectrometry

Rebecca S. Glaskin, Stephen J. Valentine, and David E. Clemmer*

Department of Chemistry, Indiana University, Bloomington, Indiana 47405

A new operational mode for an ion cyclotron mobility spectrometry instrument is explored as a possible means of performing high-resolution separations. The approach is based on oscillating fields that are applied to segmented regions of a circular drift tube. Ions with mobilities that are resonant with the frequency of field application are transmitted while nonresonant species are eliminated. An ion mobility spectrum is obtained by scanning the drift field application frequency. The approach is demonstrated by examining mixtures of ions produced by electrospraying the substance P peptide, as well as a mixture of tryptic peptides obtained by enzymatic digestion of cytochrome *c*. Drift field application frequency scans of substance P peptide ions show that it is possible to separate [M+2H]$^{2+}$ ions, and compact and elongated forms of [M+3H]$^{3+}$ ions. The resolution of different ions is related to the number of cycles for the analysis. At high cycle numbers (>50 3/4 or a drift length of 9242.03 cm) values of the resolving power can exceed 300 with a maximum resolving power of ~400. The ability to tune the resolving power of a mobility-based separation by varying the ion cycle number has substantial analytical utility.

Ion mobility spectrometry (IMS) has emerged as an important means of separating and characterizing the structures of ions. One limiting feature of the approach is its limited ability to resolve different species. The resolving power (R) is given by eq 1.[1]

$$R = \frac{t_D}{\Delta t} \approx \left(\frac{LEze}{16 k_b T \ln 2} \right)^{1/2} \quad (1)$$

In this equation, t_D corresponds to an ion's drift time and Δt is the peak width at half-maximum; ze and k_b correspond to the ion's charge and Boltzmann's constant, respectively; the variables T, L, and E correspond to the experimental buffer gas temperature, drift region length, and electric field, respectively. While this equation shows that it is possible to improve experimental resolving power by increasing values of E and L, or, by decreasing T, the square root dependence of the resolving power on these variables makes obtaining very high resolution separations technically difficult. Currently, many instruments are capable of generating spectra having $R = 10$

to 50;[2−7] a few high-resolution instruments are capable of separating ions with resolving powers in the range of ~100 to 200.[8−16]

Recently, we developed a segmented drift tube that is capable of separating a continuous beam of ions by using modulated drift fields.[17,18] In this approach, referred to as overtone mobility spectrometry (OMS), ions are stable when the drift field application frequency (and other conditions of the experiment) leads to a resonance with different ions' mobilities. Initial experiments showed that the ability to resolve peaks scales roughly in a linear fashion with the number of drift region segments (i.e., directly proportional to the overall drift region length, instead of the square root relationship mentioned above). Simple theoretical considerations led to eq 2, which describes the resolving power (R_{OMS}) of this approach,[18]

$$R_{OMS} = \frac{1}{1 - \left[1 - \dfrac{C_2}{R_{IMS}} \right] \left[\dfrac{mn - \left[\phi - 1 - \dfrac{l_e}{l_t + l_e} \right]}{mn} \right]} \quad (2)$$

In eq 2 the variables m, n, Φ, and C_2 correspond to the OMS experimental parameters, the harmonic index, the number of segmented drift (d) regions, the experimental phase (number

(1) Revercomb, H. E.; Mason, E. A. *Anal. Chem.* **1975**, *47*, 970–983.
(2) Wyttenbach, T.; von Helden, G.; Bowers, M. T. *J. Am. Chem. Soc.* **1996**, *118*, 8355–8364.
(3) Liu, Y.; Valentine, S. J.; Counterman, A. E.; Hoaglund, C. S.; Clemmer, D. E. *Anal. Chem.* **1997**, *69*, 728A–735A.
(4) Fernandez-Lima, F. A.; Becker, C.; McKenna, A. M.; Rodgers, R. P.; Marshall, A. G.; Russell, D. H. *Anal. Chem.* **2009**, *81*, 9941–9947.
(5) Kwasnik, M.; Fuhrer, K.; Gonin, M.; Barbeau, K.; Fernandez, F. M. *Anal. Chem.* **2007**, *79* (20), 7782–7791.
(6) Kanu, A. B.; Gribb, M. M.; Hill, H. H. *Anal. Chem.* **2008**, *80*, 6610–6619.
(7) Albrieux, F.; Calvo, F.; Chirot, F.; Vorobyev, A.; Tsybin, Y. O.; Lepère, V.; Antoine, R.; Lemoine, J.; Dugourd, P. *J. Phys. Chem. A* **2010**, *114*, 6888–6896.
(8) Dugourd, Ph.; Hudgins, R. R.; Clemmer, D. E.; Jarrold, M. F. *Rev. Sci. Instrum.* **1997**, *68*, 1122–1129.
(9) Wu, C.; Siems, W. F.; Asbury, G. R.; Hill, H. H. *Anal. Chem.* **1998**, *70*, 4929–4938.
(10) Asbury, G. R.; Hill, H. H. *J. Microcolumn Sep.* **2000**, *12*, 172–178.
(11) Tang, K.; Shvartsburg, A. A.; Lee, H.; Prior, D. C.; Buschbach, M. A.; Li, F.; Tomachev, A.; Anderson, G. A.; Smith, R. D. *Anal. Chem.* **2005**, *77*, 3330–3339.
(12) Koeniger, S. L.; Merenbloom, S. I.; Valentine, S. J.; Udseth, H.; Smith, R. D.; Clemmer, D. E. *Anal. Chem.* **2006**, *78*, 4161–4174.
(13) Merenbloom, S. I.; Koeniger, S. L.; Valentine, S. J.; Plasencia, M. D.; Clemmer, D. E. *Anal. Chem.* **2006**, *78*, 2802–2809.
(14) Gillig, K. J.; Ruotolo, B. T.; Stone, E. G.; Russell, D. H. *Int. J. Mass Spectrom.* **2004**, *239*, 43–49.
(15) Kemper, P. R.; Dupuis, N. F.; Bowers, M. T. *Int. J. Mass Spectrom.* **2009**, *287*, 46–57.

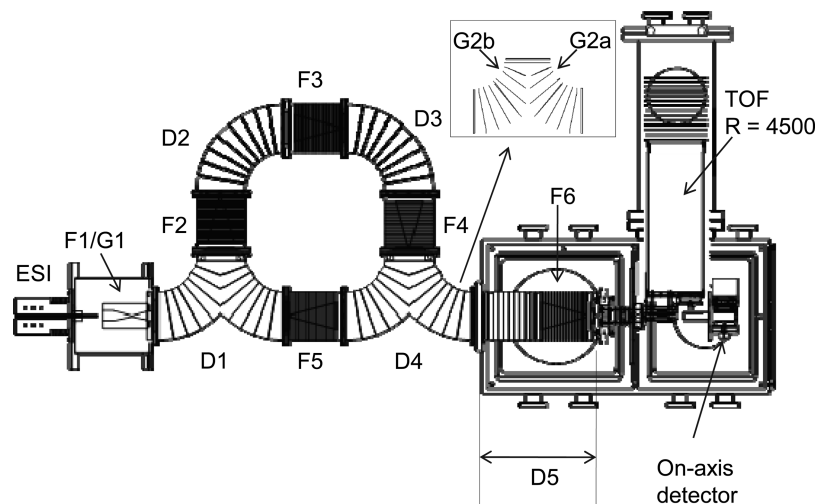* To whom correspondence should be addressed.

Figure 1. Schematic diagram of the IMS-MS instrument with a circular drift tube. A blowup of the forked regions of the circular drift tube is shown as an inset.

of unique drift field settings), and a constant required for comparison with the IMS resolving power (R_{IMS}), respectively. Here, R_{IMS} can be represented by eq 1 where the drift length is obtained by summing the lengths of all d regions. The variables l_e and l_t correspond to the lengths of the two components comprising a single d region.

While OMS is at an early stage, follow-up studies suggested that very high resolving powers might be obtained by employing large numbers of d regions. The work presented here incorporates this type of separation using a cyclical drift tube,[19] which in theory could enable the use of any number of drift region segments (simply by varying the number of times that ions are transmitted around the circle). We refer to ion mobility measurements that involve many cycles around a drift region as ion cyclotron mobility measurements; however, no magnetic fields are used in the manipulation of ion trajectories.[19] We explore this methodology by examining ions obtained by electrospraying the simple peptide substance P, as well as a more complicated mixture of peptides, obtained from digestion of the model protein cytochrome *c* with trypsin. We find that it is relatively straightforward to obtain high resolving powers. However, under such experimental conditions, there is currently a substantial loss in signal.

The present work is related to a number of mobility-based scanning methods that have emerged in the past few years. The most prominent of these are the field asymmetric (FA)IMS[20−23] approach, which separates species due to differences in their low-field and high-field mobilities, and the long-standing differential

mobility analysis[24−28] approach, used primarily as a means of sizing particles. The FAIMS approach has recently produced spectra showing resolving powers approaching 200 for multiply charged peptide ions.[29] One important distinction of the present work and other scanning methods is that although this is a scanning approach, the operation of the system in the low-field limit and with a static gas flow allows absolute values for mobilities and cross sections to be directly determined. Thus, the results that are obtained can be compared directly with other IMS measurements.

EXPERIMENTAL SECTION

General. A schematic diagram of the instrument used in these studies is shown in Figure 1. Discussions of IMS and OMS theory and instrumentation, as well as methods of producing and detecting ions, are described elsewhere.[1,17−19,30−46] Briefly, in these experiments, electrospray ionization (ESI)[47] is used to generate a constant beam of ions. Unlike the continuous beam operation mode of OMS,[17] the circular configuration used here requires that experiments are initiated by a pulse of ions. Thus, to initiate experiments, the continuous ESI beam is trapped using a Smith-geometry ion funnel[48] and an electrostatic gate (G1) and periodically packets of ions (150 μs wide) are introduced into the circular geometry drift tube by simply dropping the G1 trapping potential. The pulse used to activate the G1 introduction gate is synchronized to: (1) a data acquisition system (described previously); (2) the drift field frequency wavedriver (used to provide the time dependent fields that move ions around the circle (also

(16) Srebalus, C. A.; Li, J.; Marshall, W. S.; Clemmer, D. E. *Anal. Chem.* **1999**, *71*, 3918–3927.

(17) Kurulugama, R.; Nachtigall, F. M.; Lee, S.; Valentine, S. J.; Clemmer, D. E. *J. Am. Soc. Mass Spectrom.* **2009**, *20*, 729–737.

(18) Valentine, S. J.; Stoke, S. T.; Kurulugama, R.; Nachtigall, F. M.; Clemmer, D. E. *J. Am. Soc. Mass Spectrom.* **2009**, *20*, 738–750.

(19) Merenbloom, S. I.; Glaskin, R. S.; Henson, Z. B.; Clemmer, D. E. *Anal. Chem.* **2009**, *81*, 1482–1487.

(20) Gorshkov, M. P. *U.S.S.R. Inventor's Certificate 966583*, 1982.

(21) Purves, R. W.; Guevremont, R.; Day, S.; Pipich, C. W.; Matyjaszczyk, M. S. *Rev. Sci. Instrum.* **1998**, *69*, 4094–4105.

(22) Guevremont, R. *J. Chromatogr. A* **2004**, *1058*, 3–19.

(23) Shvartsburg, A. A.; Tang, K.; Smith, R. D. *Anal. Chem.* **2004**, *76*, 7366–7374.

(24) Rosell-Llompart, J.; Loscertales, J. G.; Bingham, D.; Fernandez,de la Mora, J. *J. Aerosol Sci.* **1996**, *27*, 695–719.

(25) Kaufman, S. L.; Skogen, J. W.; Dorman, F. D.; Zarrin, F.; Lewis, K. C. *Anal. Chem.* **1996**, *68*, 1895–1904.

(26) Mouradian, S.; Skogen, J. W.; Dorman, F. D.; Zarrin, F.; Kaufman, S. L.; Smith, L. M. *Anal. Chem.* **1997**, *69*, 919–925.

(27) Loo, J. A.; Berhane, B.; Kaddis, C. S.; Wooding, K. M.; Xie, Y. M.; Kaufman, S. L.; Chernushevich, I. V. *J. Am. Soc. Mass Spectrom.* **2005**, *16* (7), 998–1008.

(28) Kaddis, C. S.; Lomeli, S. H.; Yin, S.; Berhane, B.; Apostol, M. I.; Kickhoefer, V. A.; Rome, L. H.; Loo, J. A. *J. Am. Soc. Mass Spectrom.* **2007**, *18*, 1206–1216.

(29) Shvartsburg, A. A.; Danielson, W. F.; Smith, R. D. *Anal. Chem.* **2010**, *82*, 2456–2462.

described previously);[17−19] and, (3) the exit gate (used to direct ions out of the circle and into the mass spectrometry detection region).

Upon leaving the source, the ion packet enters a short curved region (called an "on ramp") that transmits ions into the main body of the circular drift tube. The drift tube contains eight distinct segments: four curved regions (labeled D1 to D4), each with a length of 30.01 cm; two sections (D1 and D4) have Y-shaped geometries; and four ion funnels (labeled F2 to F5), each with a length of 15.21 cm. The drift field across each region is established with a series of resistors (5 MΩ for each curve, 1.5 MΩ for each funnel) used as voltage dividers. Ions in the D4 region are controlled using electrostatic gates, with the lenses in the center of the Y being split as displayed in the inset in Figure 1. Lenses labeled G2a and G2b are isolated from the resistor chain and with the appropriate applied voltages it is possible to maintain ions in the circle for multiple passes (cycles) or to release them to the detector.

The drift field is controlled by a square wave at a fixed frequency generated from a home-built pulsing system (wavedriver).[17−19] A packet of ions is propagated around the drift tube with the injection pulse (G1) occurring with the first field application setting (phase A). Within the field application time frame, ions can move into the D1 region but a large repulsive field at the end of this region and the beginning of the F2 region prevents the ions from moving any further. Once the field switches to the second application setting (phase B), ions can move from the D1 region into the F2 region. Ions not entering the F2 region

before the next phase A field application setting are eliminated as the large repulsive potential (D1 to F2) prevents them from entering this region and they diffuse to surrounding electrodes and are neutralized. Due to a large repulsive potential at the F2/D2 junction, ions at the leading edge of the distribution are defocused and also diffuse to surrounding electrodes. During the next field application cycles (A → B → A), ions travel from the F2 region to the F3 region. Switching the potential in this manner eliminates ions at the leading and trailing edge as described above. This ensures that only ions with mobilities allowing them to travel one D region and one F region during a field application cycle are transmitted around the circular drift tube. Ions are maintained within the circular drift tube using the appropriate voltage settings applied to the split lens assembly (G2a/G2b in Figure 1) at delay times that are multiples of the wavedriver period.

As a result of the applied voltages, there are four ion transmission (d_t) and four ion elimination (d_e) regions any time within the instrument. The d_t regions in the circular instrument are significantly smaller than the d_e regions. With respect to the applied drift field, during a full cycle (time period of the A → B → A transition) of the wavedriver, ions travel ∼45.22 cm to remain stable within the circle. This corresponds to one d region which is the length of a single d_t (funnel) and a single d_e (curve) region. In one complete cycle, ions travel 180.88 cm.

A drift field of 7 V·cm^{-1} is applied across each of the drift regions and ion funnels in the circular portion of the drift tube. The linear region (D5 and F6) is 32.35 cm and utilizes a field of 9 V·cm^{-1}. F1 is operated at a field of 20.6 V·cm^{-1} with an rf frequency of 425 kHz (90 Vp-p). F6 is operated at a frequency of 234 kHz (228 Vp-p). All other funnels are operated with an rf frequency of 230 kHz (130 Vp-p). After completing the desired number of cycles around the drift tube, a gating voltage is applied to the split lens assembly (G2a/G2b in Figure 1) to extract ions from the circular drift tube and send them to the drift tube exit orifice. Ions are subsequently focused through a series of ion optics before being mass analyzed and detected. The entire drift tube is maintained at pressure of 3.20 ± 0.01 Torr He at 300 K, with the pressure being monitored by a capacitance manometer.

Reduced mobilities (K_0) are determined from the expression:[17,18]

$$K_0 = \frac{f(l_t + l_e)}{E} \frac{P}{760} \frac{273.2}{T} \tag{3}$$

In eq 3, the variables P and f correspond to the pressure of the buffer gas and the frequency of the wavedriver (drift field application frequency), respectively.

Electrospray Conditions. A substance P (Sigma, 95% purity) solution (10^{-4} M in 49:49:2 water:ACN:acetic acid by volume) was used without further purification. Cytochrome c (equine, >90% purity) was purchased from Sigma Aldrich. The tryptic digestion was obtained by dissolving 10 mg of cytochrome c protein in a 500 μL buffer solution of 100 mM ammonium bicarbonate with 6 M urea (pH 8.0). The protein was allowed to denature for 1 h and 1.0 mL of buffer solution (100 mM ammonium bicarbonate) was added to the denatured protein to reduce the urea concentration. A 100 μL aliquot of a stock trypsin solution was added to the protein solution to provide a trypsin:protein ratio of 1:50 (wt./wt.). Digestion was carried

(30) Mack, E. *J. Am. Chem. Soc.* **1925**, *47*, 2468−2482.

(31) Mason, E. A.; McDaniel; E. W. *Transport Properties of Ions in Gases*; Wiley: New York, 1988.

(32) Shvartsburg, A. A.; Jarrold, M. F. *Chem. Phys. Lett.* **1996**, *261*, 86−91.

(33) Mesleh, M. F.; Hunter, J. M.; Shvartsburg, A. A.; Schatz, G. C.; Jarrold, M. F. *J. Phys. Chem.* **1996**, *100*, 16082−86.

(34) Wyttenbach, T.; von Helden, G.; Batka, J. J.; Carlat, D.; Bowers, M. T. *J. Am. Chem. Soc.* **1997**, *8*, 275−82.

(35) Koeniger, S. L.; Merenbloom, S. I.; Clemmer, D. E. *J. Phys. Chem B* **2006**, *110*, 7017−7021.

(36) Wittmer, D.; Luckenbill, B. K.; Hill, H. H.; Chen, Y. H. *Anal. Chem.* **1994**, *66*, 2348−2355.

(37) Gillig, K. J.; Ruotolo, B.; Stone, E. G.; Russell, D. H.; Fuhrer, K.; Gonin, M.; Schultz, A. *J. Anal. Chem.* **2000**, *72*, 3965−3971.

(38) Hoaglund, C. S.; Valentine, S. J.; Sporleder, C. R.; Reilly, J. P.; Clemmer, D. E. *Anal. Chem.* **1998**, *70*, 2236−2242.

(39) Hoaglund-Hyzer, C. S.; Li, J.; Clemmer, D. E. *Anal. Chem.* **2000**, *72*, 2737−2740.

(40) Valentine, S. J.; Kulchania, M.; Barnes, C. A. S.; Clemmer, D. E. *Int. J. Mass Spectrom.* **2001**, *212*, 97−109.

(41) Tang, K.; Shvartsburg, A. A.; Lee, H. N.; Prior, D. C.; Buschbach, M. A.; Li, F. M.; Tolmachev, A. V.; Anderson, G. A.; Smith, R. D. *Anal. Chem.* **2005**, *77*, 3330−3339.

(42) Koeniger, S. L.; Merenbloom, S. I.; Valentine, S. J.; Jarrold, M. F.; Udseth, H. R.; Smith, R. D.; Clemmer, D. E. *Anal. Chem.* **2006**, *78*, 4161.

(43) Merenbloom, S. I.; Koeniger, S. L.; Valentine, S. J.; Plasencia, M. D.; Clemmer, D. E. *Anal. Chem.* **2006**, *78*, 2802−2809.

(44) For a review of IMS techniques see (and references therein): St. Louis, R. H.; Hill, H. H. *Crit. Rev. Anal. Chem* **1990**, *21*, 321−355.

(45) For a review of IMS techniques see (and references therein): Clemmer, D. E.; Jarrold, M. F. *J. Mass Spectrom* **1997**, *32*, 577−592.

(46) For a review of IMS techniques see (and references therein): Bohrer, B. C.; Merenbloom, S. I.; Koeniger, S. L.; Hilderbrand, A. E.; Clemmer, D. E. *Annu. Rev. Anal. Chem* **2008**, *1* (10), 1−10.

(47) Fenn, J. B.; Mann, M. L.; Meng, C. K.; Wong, S. F.; Whitehouse, C. M. *Science* **1989**, *246*, 64−71.

(48) (a) Shaffer, S. A.; Tang, K. Q.; Anderson, G. A.; Prior, D. C.; Udseth, H. R.; Smith, R. D. *Rapid Commun. Mass Spectrom.* **1997**, *11*, 1813−1817. (b) Shaffer, S. A.; Prior, D. C.; Anderson, G. A.; Udseth, H. R.; Smith, R. D. *Anal. Chem.* **1998**, *70*, 4111−4119.
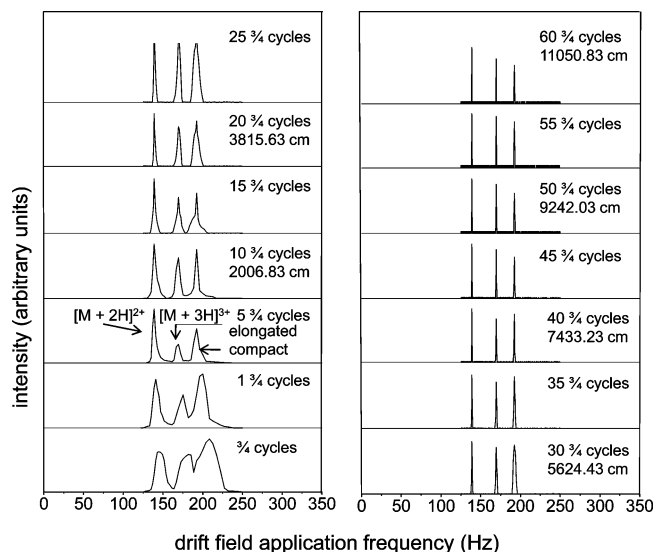
Figure 2. Drift field application frequency distribution plots at different cycle numbers. Features representing the [M + 2H]²⁺ charge state and two conformations of the [M + 3H]³⁺ charge state ions are labeled. Drift region lengths are provided for several of the experiments.

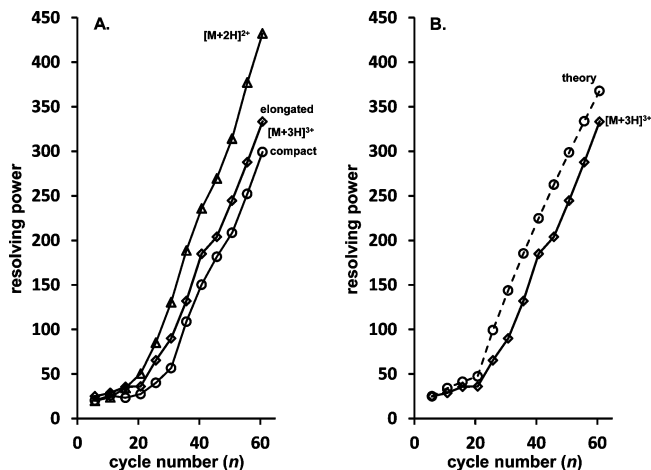**Figure 3.** (A) Resolving power, $f/\Delta f$(FWHM), obtained for substance P ions at different cycle numbers. Open triangles, open diamonds, and open circles correspond to [M + 2H]²⁺, elongated [M + 3H]³⁺, and compact [M + 3H]³⁺ ions. (B) Comparison of experiment and theory for resolving power dependence on cycle number. Open diamonds correspond to the elongated [M + 3H]³⁺ ions. Open circles correspond to a fit to the data, where $f/\Delta f$ scales with the square root of the number of cycles at short drift tube lengths (5 3/4 to 15 3/4 cycles) and according to eq 2 at larger cycle numbers. See text for details.

out for a 24 h period in a 37 °C water bath. Digested peptides were desalted using solid phase extraction (HLB Oassis Cartridges, Waters) and subsequently lyophilized. Digest peptides were dissolved in 1.0 mL of 49:49:2 water:ACN:acetic acid solution. Ions were formed by infusing (0.40 μL·min⁻¹) either solution through a pulled tip capillary maintained at a dc bias of 2000 V above the ESI source entrance aperture.

RESULTS AND DISCUSSION

Elimination of Ion Transmission Ion Overtone Regions. One complication of the OMS approach is that a species with a single mobility may appear at multiple frequencies across the field application frequency scan.[17,18] For a mixture of ions, this overlap of different overtone regions can result in confusing spectra. To simplify the present data, we focus on only the fundamental frequency region of the spectrum. Because overtones depend upon the ratio of the lengths of the d_e and d_t regions, it is possible to eliminate them by making the d_t region much smaller than that of d_e. In the present design, $l_t = 15.21 \ll l_e = 30.01$ cm. Thus all peaks in the data shown below correspond to the fundamental frequency region. Additionally, each single ion structure should yield only a single peak across the frequency range that is employed.

Experimental Drift Field Application Frequency Distributions. Figure 2 shows the frequency distribution plots for substance P ions for experiments employing different numbers of cycles around the circular drift tube. After traversing ∼3/4 of the circular drift tube (198.03 cm), three prominent features are observed. In the lower frequency region, a single feature centered at 140 Hz is resolved. This peak has a m/z value of 674.80 and has been assigned as [M + 2H]²⁺ substance P ions. Two unresolved peaks centered at 180 and 212 Hz are also observed. These features each have a m/z value of 450.22 and have been assigned to elongated and compact forms, respectively, of [M + 3H]³⁺ substance P ions. Increasing the number of cycles produces narrower peaks for all species. By 5 3/4 cycles

(1102.43 cm), all three peaks are baseline resolved. The resolution of the measurement continues to improve with increasing numbers of cycles. For example, after 40 3/4 (7433.23 cm), 50 3/4 (9242.03 cm), and 60 3/4 (11050.83 cm) cycles, the resolving power derived from the peak corresponding to the [M+2H]²⁺ ions is 240, 310, and 430, respectively.

Reduced mobilities can be determined for these data set features using the peak frequencies and eq 3. For example, the peak frequency obtained for the [M + 2H]²⁺ substance P ions is 137.5 Hz after 60 3/4 cycles. From eq 3, this corresponds to K_0 = 3.41 cm²·V⁻¹·s⁻¹. This value is within 0.2% of the value determined for [M + 2H]²⁺ substance P ions from measurements with a linear drift tube.[49] Reduced mobilities corresponding to the compact and elongated conformations of the [M + 3H]³⁺ substance P ions are 4.11 and 4.76 cm²·V⁻¹·s⁻¹, respectively.

Figure 3A summarizes the dependence of the resolving power on the number of cycles the ions travel around the circular drift tube. These values have been obtained from the distributions shown in Figure 2. For the [M + 2H]²⁺ substance P ions, the resolving power increases gradually from a value of 20 to 34 for cycle numbers of 5 3/4 and 15 3/4 (2911.23 cm), respectively. Above 15 3/4 cycles, the resolving power improves dramatically beginning with a value of 50 at 20 3/4 cycles (3815.63 cm). Higher resolving powers are observed for increased cycle numbers. A maximum value of 430 is reached at 60 3/4 cycles. The same trends are observed for the elongated and compact conformations of the [M + 3H]³⁺ substance P ions. A difference is the transition region over which a greater rate of increase in resolving power is observed.

(49) Myung, S.; Lee, Y. J.; Moon, M. H.; Taraszka, J.; Sowell, R.; Koeniger, S.; Hilderbrand, A. E.; Valentine, S. J.; Cherbas, L.; Cherbas, P.; Kaufmann, T. C.; Miller, D. F.; Mechref, Y.; Novotny, M. V.; Ewing, M. A.; Sporleder, C. R.; Clemmer, D. E. *Anal. Chem.* **2003**, *75* (19), 5137–5145.
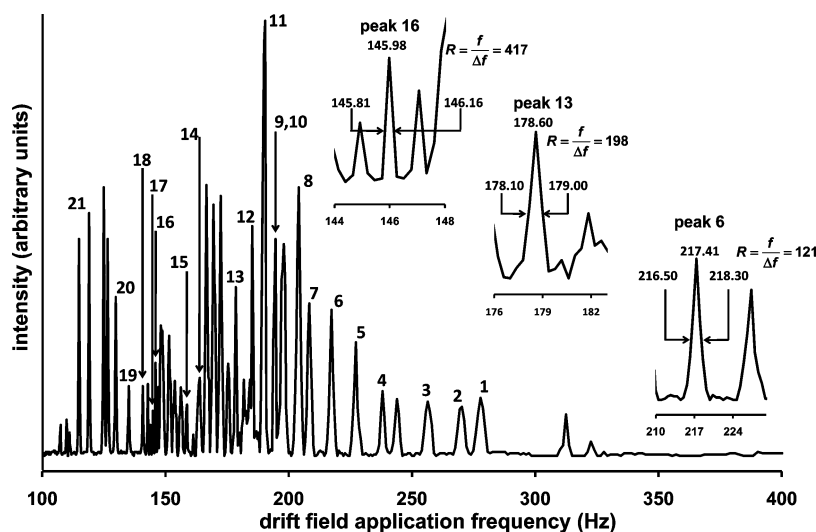
Figure 4. Drift field application frequency distribution obtained for a cytochrome *c* digest. Identified peptide ions are labeled according to the peak numbers provided in Table 1. Three peaks showing the range of resolving power values that are obtained from an analysis of this data set are shown on an expanded drift field application frequency scale.

For the elongated and compact conformations of the $[M + 3H]^{3+}$ substance P ions, this transition occurs above ~20 3/4 cycles.

It is instructive to consider the origin of the resolving power dependence on cycle number. One scenario for the two separate rates of increase is that at lower cycle numbers, the resolving power scales as the square root of the overall drift length. It is possible that this dependence is related to the diffusion of the initial 150 μs-wide ion packet. That is, the root-mean-square displacement of an ion due to diffusion is proportional to the square root of the product of the diffusion coefficient and time. In this scenario, the small pulse of ions must diffuse to occupy a full d_t region prior to being subject to the ion elimination (mobility trimming) effect described above. Thus, ions of very similar mobilities would not easily be distinguished until the ion packet diffused to the size of a funnel region (Figure 1). Once the ion cloud has diffused to the size of a d_t region, the mobility discrimination becomes more pronounced leading to the greater increase in resolving power with drift length. This is similar to the process that occurs with OMS measurements. Previous theoretical work has shown that, for OMS measurements, the resolving power is directly proportional to the number of d regions employed in the drift tube.[17,18]

Figure 3B shows a theoretical trace consisting of two separate functions. Here the initial experimental resolving power at 5 3/4 cycles is allowed to scale as the square root of cycle number (effectively drift tube length) to 15 3/4 cycles. Above 15 3/4 cycles, eq 2 is used to determine the OMS contribution to the overall resolving power which is added to the base value (15 3/4 cycles) for higher cycle numbers. For these calculations, the OMS parameters m and Φ are 1 and 2, respectively. The value n represents the number of d regions the ions traverse during the measurement (i.e., n = cycle number × 4 + 3). Values of 15.20 and 30.01 cm have been used for l_t and l_e, respectively. R_{IMS} is calculated from eq 1 using a value of 300 K as a buffer gas temperature and a total drift length of $n \cdot (l_t + l_e)$. In the comparison of theory with the experimental results for the

$[M + 3H]^{3+}$ elongated ions (Figure 3B), the agreement at low cycle numbers is good with very similar values obtained from the fit to the data. Above 15 3/4 cycles, use of eq 2 results in a relatively good fit to the experimental data as well. Similar rates of increasing resolving power with cycle number are observed for both the theoretical and experimental data points. On average, the theoretical data points are offset to higher values of resolving power by ~47 ± 10. Here we note that in general, use of eq 2 slightly overestimated the resolving power of linear OMS drift tubes as well.[18]

Separation of a Mixture of Tryptic Peptides. Figure 4 shows a distribution obtained upon electrospraying a tryptic digest of the protein cytochrome *c*. At least 45 distinct features are observed in the distribution. The majority of the data set features observed occur between 100 and 200 Hz. Above 200 Hz, several features corresponding to ions with the highest mobilities are observed. To identify the peptides represented in the frequency distribution, the same sample has been analyzed using IMS-MS techniques (data not shown here). Consider peak 18 in Figure 4 located at 140.85 Hz. From eq 3, $K_0 = 3.49$ cm$^2 \cdot$V$^{-1} \cdot$s^{-1} for this feature. From the IMS-MS analysis of the same tryptic digest, a peak having $m/z = 748.28$ is observed with a drift time corresponding to $K_0 = 3.45$ cm$^2 \cdot$V$^{-1} \cdot$s^{-1} and has been assigned to the [EETLMEYLENPK+2H]$^{2+}$ ion. Although the IMS-MS data is not shown here, we note that this K_0 value corresponds to a collision cross section that is within 1% of that reported previously for this peptide.[50] As another example, peak 3 has a reduced mobility that is very similar (6.35 versus 6.45 cm$^2 \cdot$V$^{-1} \cdot$s^{-1}) to that obtained for a peak having $m/z = 604.26$ in the IMS-MS data set. This feature has been assigned to the peptide ion [GITWK + 2H]$^{2+}$. Table 1 contains a list of all assigned tryptic peptide ions with corresponding drift field application periods ($1/f$) and reduced mobilities. Of the 21 peptides

(50) Valentine, S. J.; Counterman, A. E.; Clemmer, D. E. *J. Am. Soc. Mass Spectrom.* **1999**, *10*, 1188–1211.

Table 1. Reduced Mobilities for Cytochrome *c* Tryptic Peptide Ions

sequence[a]	z	period (ms)[b]	K_0 circular[c]	K_0 IMS[d]	peak[e]
KATNE	2	3.6	6.88	6.90	1
KTER	2	3.7	6.70	6.67	2
GITWK	2	3.9	6.35	6.45	3
IFVQK	2	4.2	5.90	5.91	4
YIPGTK	2	4.4	5.63	5.71	5
HK	1	4.6	5.39	5.45	6
TGPNLHGLFGR	3	4.8	5.16	5.10	7
MIFAGIK	2	4.9	5.06	5.10	8
CAQCHTVEK-HEME	3	5.1	4.82	4.77	9
KTGQAPGFTYTDANK	3	5.1	4.82	4.77	10
MIFAGIKK	2	5.2	4.72	4.70	11
HKTGPNLHGLFGR	3	5.4	4.59	4.52	12
EDLIAYLK	2	5.6	4.42	4.47	13
TGPNLHGLFGR	2	6.1	4.06	4.02	14
GITWKEETLMEYLENPK	3	6.3	3.93	3.95	15
TGQAPGFTYTDANK	2	6.8	3.67	3.62	16
TEREDLIAYLK	2	6.9	3.59	3.54	17
EETLMEYLENPK	2	7.1	3.49	3.45	18
EETLMEYLENPKK	2	7.4	3.35	3.37	19
GITWK	1	7.7	3.21	3.21	20
IFVQK	1	8.4	2.95	2.99	21

[a] Peptide ion sequences as obtained from the Swiss-Prot database. Assignments are made by matching mobilities with features assigned in IMS-MS data sets obtained for the same sample. [b] Field application periods have been determined from the data set collected using 60 3/4 cycles (Figure 4). [c] Reduced mobilities ($cm^2*V^{-1}s^{-1}$) obtained using the drift field application frequency from Figure 4 and eq 3. [d] Reduced mobilities obtained for assigned peptides in an IMS-MS data set (data not shown). [e] Labels for peaks observed in Figure 4.

assigned in Table 1, 15 have been identified previously using injected-ion drift tube instruments.[50,51] All peptides not previously identified are products of missed cleavages, indicating that they may be unique to this sample as a result of differing efficiencies in enzymatic digestion.

The resolving power for the features observed in the frequency distribution shown in Figure 4 range from ∼50 to ∼400, as illustrated by the insets in Figure 4 representing several of the assigned peaks. The lower values—compared with that obtained for substance P ions—may result from chemical noise. That is, for a mixture of even moderate complexity, many species exhibit significant overlap in mobilities. This presents a challenge, as some peaks will not appear to become narrower with increasing resolving power until after reaching the threshold of component resolution. This problem is not so unlike that encountered by mass spectrometers with resolving powers approaching that required to achieve isotopic resolution. It should also be noted that some of the interfering species may arise from ions exhibiting multiple gas-phase conformations. Thus, the peaks of vastly different widths observed in Figure 4 may be indicative of incomplete resolution of many different ion structures.

CONCLUSIONS

A frequency scanning method for ion cyclotron mobility spectrometry measurements has been described. Overall, it appears relatively straightforward to generate high-resolution spectra. Peaks indicating resolving powers in excess of 400 have been observed. A separation of components from a peptide mixture produced by tryptic digestion of cytochrome *c* using the frequency scanning method has been presented. Resolving power, determined from peptide ion peaks, ranges from ∼50 to ∼400. The work presented here represents the most efficient mobility separation to date of a protein digest mixture. A limitation of the ion cyclotron mobility spectrometry measurements as described here is that increased resolution comes at a cost to sensitivity. Current work in our laboratory, involving ion trapping, focusing, and multiplexing techniques is aimed at improving the sensitivity of the approach.

(51) Henderson, S. C.; Valentine, S. J.; Counterman, A. E.; Clemmer, D. E. *Anal. Chem.* **1999**, *71*, 291–301.